Materials Chemistry and Physics 219 (2018) 292–302

Contents lists available at ScienceDirect

Materials Chemistry and Physics

journal homepage: www.elsevier.com/locate/matchemphys

Wettability transition on micro-nano hierarchical structured Ni20Cr coating surface by selective spontaneous adsorption during vacuum evacuation

Jie Li, Chengxin Li*, Guanjun Yang, Changjiu Li

State Key Laboratory for Mechanical Behavior of Materials, School of Materials Science and Engineering, Xi'an Jiaotong University, Xi'an, Shaanxi, 710049, PR China

HIGHLIGHTS

- A biomimetic micro-nano structured surface was constructed by plasma spraying.
- Ni20Cr surface can rapidly obtain super-hydrophobicity under vacuum evacuation.
- Saturated hydrocarbon-based residual gas was present in oil-free vacuum systems.
- Selective spontaneous adsorption played main role in wettability transition.
- The reversible wettability transition occurred through vacuum and UV-O_3 treatment.

ARTICLE INFO

Keywords:
Shrouded plasma spraying
Micro-nano structure
Super-hydrophobicity
Vacuum
Wettability transition

ABSTRACT

A coating surface of metallic Ni20Cr with a bionic hierarchical micro-nano scaled structure was fabricated by shrouded plasma spraying technology. A novel phenomenon was found on the coating surface that the surface wettability can change from original super-hydrophilicity to super-hydrophobicity with a contact angle of 152° and sliding angle of 2° by evacuation in oil-free vacuum systems. To clarify the wettability transition mechanism in vacuum conditions, the microstructure and chemical composition of the coating surface were systematically investigated. The results revealed that the main reason for the wettability transition was due to the formation of chemisorbed carboxylates and physisorbed saturated hydrocarbons on the coating surface by selective spontaneous adsorption of the residual gas molecules from vacuum environment. The hydrophobic saturated hydrocarbon chains oriented outward the surface effectively reduced the surface energy and cause a spontaneous wettability transition. The evacuation process under the vacuum conditions enhanced the adsorption rate on the coating surface. The degree of wettability transition depended on the amount of the surface adsorbates.

1. Introduction

Wettability is one of the most important properties of solid material surfaces. Super-hydrophobic surface with a water contact angle higher than 150° and sliding angle lower than 10° has aroused much attention [1–3]. Super-hydrophobicity is a common phenomenon present in nature, where lotus leaf surface represents the most typical matter with highly stable hydrophobicity and self-cleaning performance [4]. Through the study of lotus leaf, Feng et al. [5] proposed that the super-hydrophobicity is caused by a combination of micro-nano-fractal structure and low surface free energy wax on the surface. This means that the geometrical structure and chemical composition are the two key factors affecting the surface wettability [6].

Metals and their oxides are the most widely used engineering materials. Super-hydrophobic properties of metal and oxide surfaces have potential applications in many industrial sectors, including anti-corrosion, anti-icing, oil-water separation and so on [7–9]. The vast majority of metals and oxides have high surface energy, causing intrinsic hydrophilicity [10]. For this reason, in order to use these materials to produce super-hydrophobic surfaces, it is necessary to modify them by organic matters with low surface free energy, such as fluorosilanes and fatty acids [11,12].

It was discovered in the present study that without adding any organic matters artificially, the metallic coating surface can spontaneously switch from super-hydrophilicity to super-hydrophobicity after testing in some commonly used devices that working under oil-free high vacuum conditions, such as scanning electron microscopy and X-ray photoelectron spectroscopy. To the best of our knowledge, some preparation methods of super-hydrophobic surfaces without chemical modification were all related to vacuum conditions in recently

* Corresponding author.
E-mail addresses: crystallijie@163.com (J. Li), licx@mail.xjtu.edu.cn (C. Li), ygj@mail.xjtu.edu.cn (G. Yang), licj@mail.xjtu.edu.cn (C. Li).

https://doi.org/10.1016/j.matchemphys.2018.08.049
Received 27 July 2017; Received in revised form 17 June 2018; Accepted 19 August 2018
Available online 20 August 2018
0254-0584/

published reports. Martinez et al. [13] reported that a cerium oxide surface converted to hydrophobicity after subjecting an ion sputtering in the ultra-high vacuum XPS chamber. They attributed the phenomenon to the removal of polar groups on the surface by sputtering. Pedraza et al. [14] observed the phenomenon of long-term relaxation on the cerium oxide surface in an ultra-high vacuum. They thought the wettability transition was due to the dehydration of the surface, which minimized the surface defect and highly reduced the surface energy. Yan et al. [15] reported that a α-Fe_2O_3 film became super-hydrophobic after being exposed in a vacuum chamber, and Long et al. [16] showed that a copper surface can become hydrophobic after storage in a sealed vacuum container. They attributed the wettability transition to the adsorption of the organic oil molecules that came from mechanical vacuum pumps on the surface. Moreover, some literature showed that super-hydrophobicity obtained on the metal or oxide surface was due to the control of the surface structure [17–19]. The mechanisms used to explain the phenomenon given by the mentioned published reports were various. However, the reasons for the original hydrophilic surfaces became super-hydrophobic were aroused by the vacuum itself or the other factors were still not entirely clear.

In the current paper, shrouded plasma spraying was used for the fabrication of metallic Ni20Cr alloy coating surfaces. To investigate the mechanism related to the transition of surface wettability in vacuum devices, the morphological characteristics and chemical composition of the surfaces were systematically investigated, respectively. The objective of the study was to clarify the effect of the vacuum conditions on surface wettability transition. In addition, this study may provide some feasibility recommendations for the extensive surface preparation methods related to the vacuum system to avoid neglecting the effect of vacuum on surface wettability during the process. Furthermore, the study was also expected to provide an innovative approach to the preparation of super-hydrophobic surfaces.

2. Experimental

2.1. Materials

A commercial Ni20Cr powder (PR2111, XianDao, China) was used as the feedstock. The powder was composed mainly of spherical particles with size less than 30 μm. A 304 stainless steel plate with dimensions of $\Phi 20 \times 2$ mm was used as the substrate, which was sand-blasted and then cleaned with alcohol before coating deposition.

2.2. Preparation of the coating surface

A plasma spraying system (GDP-80, Jiujiang, China) was employed to deposit coating on the substrate. Fig. 1 shows the schematic diagram of the setting. The spraying was performed in the atmospheric environment. An Ar-H_2 plasma jet was generated at a plasma arc power of 40 kW. The flow rates of the primary gas Ar and the secondary gas H_2 were 50 L/min and 6 L/min, respectively. The powder was fed into the plasma jet using an internal powder port. N_2 was used as the powder carrier gas that was set at a flow rate of 8 L/min and the powder feed rate for coating deposition was 20 g/min. A gas shroud component with argon at a flow rate of 20 L/min was utilized to promote vaporization and minimize the oxidation of powder particles during in-flight process. When the particles were fed into the plasma jet with high temperature and high speed, they melted and then collided and deposited to form a coating on the substrate.

During the deposition process, the standoff distance from the nozzle exit to the substrate surface was 125 mm. The placement of the substrates was shown in Fig. 1b and they were kept immobile. The spray gun was controlled by a robot and ran on the set routines at a traverse speed of 50 mm/s. The average deposition time for a single substrate was about 1.6 s.

2.3. Conditions of the vacuum system

In the present study, two vacuum systems were used in the process of investigating the wettability transition of the coating surface. The entire two systems were oil-free. The first one was a vacuum system from field emission scanning electron microscopy (FESEM, MIRA3 LMH, TESCAN, Czech Republic). The vacuum chamber was evacuated by a multi-stage pump based on turbo molecular and oil-free dry pump and pumped down to a pressure of lower than 1.0×10^{-2} Pa in 5 min. The second one was a vacuum system from the X-ray photoelectron spectrometry (XPS, K-Alpha, Thermo Scientific, America). The vacuum chamber with a pressure of 3×10^{-5} Pa was evacuated by two oil-free turbo molecular pumps. During the experiment, these two different chambers were continuously evacuated to maintain the pressure.

2.4. Characterization

The morphology of coating surface was characterized by field emission scanning electron microscopy (FESEM, MIRA3 LMH, TESCAN, Czech Republic) and laser scanning confocal microscope (LSCM, VK9700K, Keyence, Japan). Surface roughness (R_a) of the coating was detected by LSCM.

Static contact angle and sliding angle measurements were carried out using a contact angle instrument (JC2000C4, Shanghai Zhongchen Digital Technic Apparatus Co., Ltd., China) under room temperature. The volume of a freshly distilled water droplet used for the measurement was 5 μL. The static contact angle was measured using a typical sessile drop method by dropping a water droplet on the surface under static condition, while the sliding angle was measured by putting a water droplet on the horizontal surface and then tilting the surface until the droplet began to move. At least five droplets were used to measure the various locations of each sample.

The diffuse reflection Fourier transform spectroscopy (DRIFTS, Vertex70, Bruker, Germany) with a resolution of 4 cm^{-1} and 128 scans

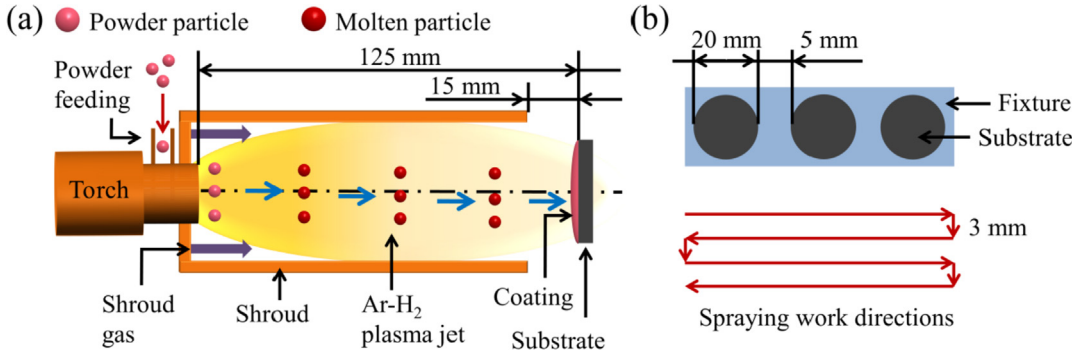

Fig. 1. Schematic diagram of shrouded plasma spraying. (a) The setting and (b) the work directions.

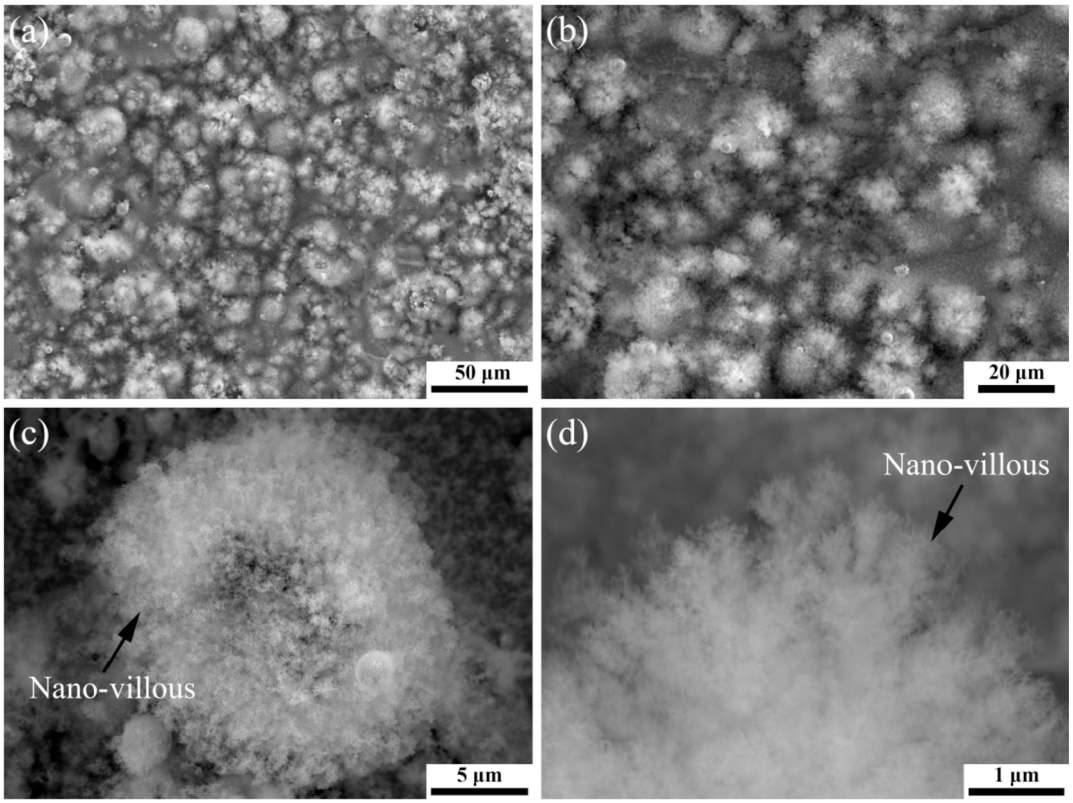

Fig. 2. Morphologies of Ni20Cr coating surface at different magnification.

was used to analyze the chemical composition of the coating surface. X-ray photoelectron spectrometry (XPS, K-Alpha, Thermo Scientific, US), in conjunction with argon ion etching (2000 eV, 10 μA), with a standard Al Kα radiation of 1486.68 eV was used to determine the content of the elements and chemical composition on the coating surface. The binding energy was calibrated using C 1s peak (284.6 eV).

UV-O_3 cleaning equipment (PSD, Novascan, US) was used to irradiate coating surface at room temperature. Low-pressure grid-Hg lamp can produce high-intensity UV light at 185 nm and 254 nm.

3. Results and discussion

3.1. Surface morphology of the Ni20Cr coating

Fig. 2a, b shows the typical surface morphology of Ni20Cr coating at the as-sprayed state. Combining with the observation of three-dimensional morphology obtained by LSCM shown in Fig. 3, it can be found that numerous micrometer-size large protrusions were randomly distributed on the coating surface. The relatively formed large protrusions were caused by the deposition of molten particles, and the smaller ones were the splashes produced by high-velocity collision of the particles. The average surface roughness was 7.7 ± 0.2 μm.

It is worth noting that a large number of uniformly and densely distributed cluster structures covered the entire coating surface, as shown in Fig. 2c, d. The cluster structures had villous-like features, and the size of them was significantly less than the original size of the feedstock particles. Further, detailed structural information of the villous-like structures was characterized using the transmission electron microscope (TEM), as shown in Fig. 4. The result showed that the villous-like structures were actually consisted of a large number of spherical nanoparticles with size less than 100 nm, and the size distribution of the nanoparticles was not uniform. As a result, the villous-like structures were nanoscale. It has been suggested that metallic elements, such as nickel and chromium, can evaporate during the high-temperature of plasma spraying and the resulting nanostructures were due to the physical deposition of the vapors [20,21]. The formation of nanostructures has been discussed in detail in the previous report [22].

Overall, the results from the morphological studies suggested that Ni20Cr based coating surface had a hierarchical structure composed of two layers: micro-potrusions and nano-villous, which is very similar to the structure of the super-hydrophobic lotus leaf surface [4,23].

3.2. Surface wettability transition in vacuum condition

The freshly as-sprayed Ni20Cr coating surface was in super-hydrophilic state that water droplet can rapidly penetrate into the surface with a contact angle of 0°. However, a reproducible unknown phenomenon was observed that the surface can switch from original super-hydrophilicity to hydrophobicity or even super-hydrophobicity after it was tested by some devices that working under high vacuum condition, such as scanning electron microscopy (SEM) and X-ray photoelectron spectroscopy (XPS).

In order to exclude the effect of the electron beams in SEM or the X-rays in XPS on surface wettability transition, the coating was only evacuated in the vacuum chamber of SEM without performing a corresponding detection step and other additional treatments. It can be seen from Fig. 5 that the surface wettability underwent a transition after evacuation, which proved that the changing in surface wettability was only related to the evacuation process under vacuum.

As can be seen from the measurement results, the varying degree of the surface wettability was depended on the different durations of evacuation. The water contact angle of the surface rapidly changed to 92.3 ± 0.8° when the evacuation time was 1 h, but the droplet cannot slide on the surface even when the coating was turned upside down, the surface was in a hydrophobic state. After 2 h of evacuation, the water contact angle on the surface reached 143.7 ± 0.4°. It is worth mentioning that the droplet can slide on the surface with a sliding angle of 16.0 ± 0.5°. By increasing the time, the surface achieved super-

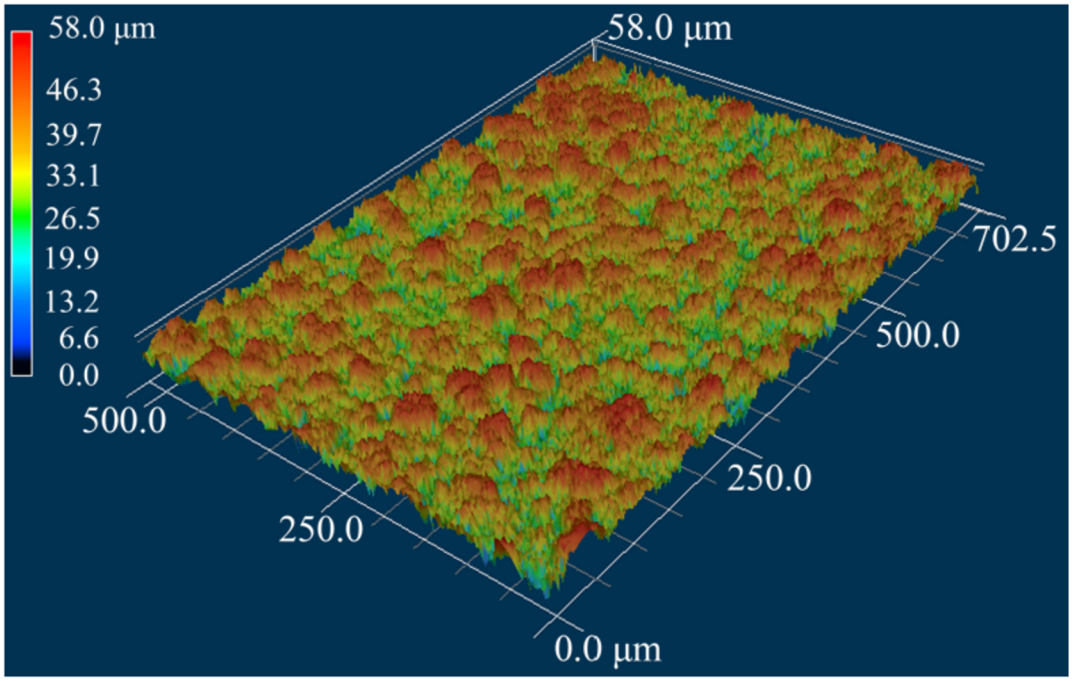

Fig. 3. Three-dimensional topography of the Ni20Cr coating surface observed by LSCM.

hydrophobic state when time reached more than 4 h. The super-hydrophobicity was pretty stable when evacuation time further incremented. The recorded surface contact angle was 152.1 ± 1.1°, and the sliding angle was 2.0 ± 0.3° when the coating was evacuated 5 h.

3.3. Surface chemical analysis

Observations showed that there was no change in surface morphology after the evacuation in the vacuum chamber of SEM. As the structure and chemical composition are the two crucial factors influencing the surface wettability, the main reason for the wettability transition was most likely related to the change in surface chemical state.

DRIFTS detection was used to get the information of chemical composition on the coating surface. The absorbance spectra of the coating surface in freshly as-sprayed state and after vacuum evacuation with different time are shown in Fig. 6.

The spectrum of freshly as-sprayed state revealed the occurrence of oxidation on the coating surface during the preparation process, where the absorption peak located below 1000 cm^{-1} was attributed to metal

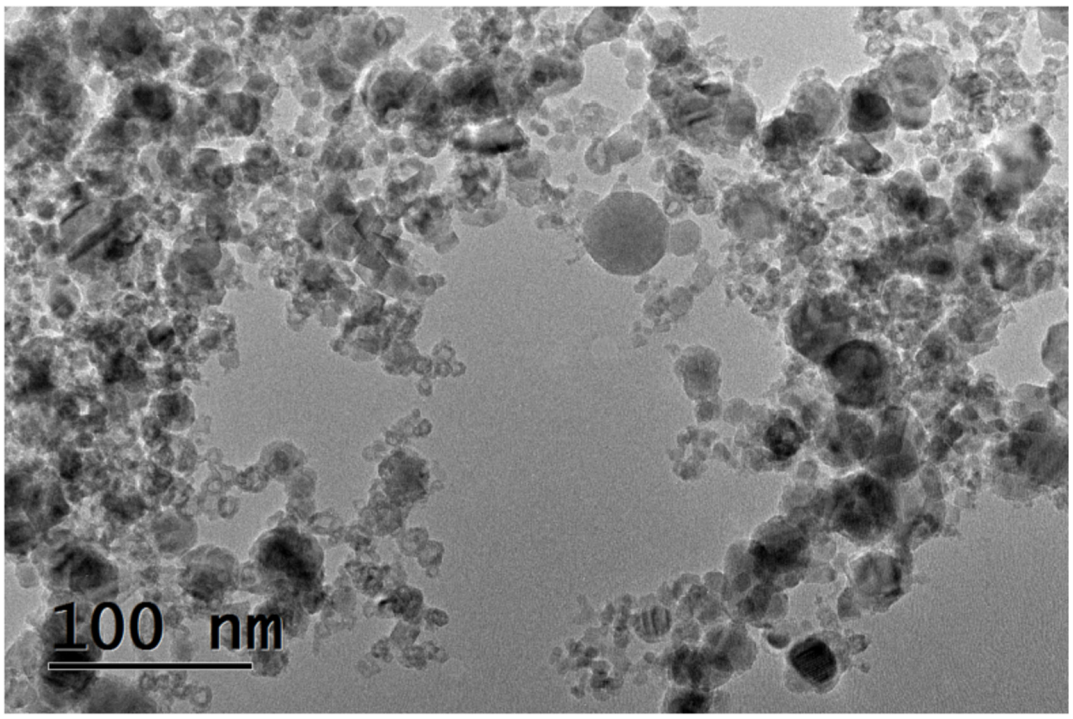

Fig. 4. TEM image of the nanoparticles that formed the villous-like cluster structures.

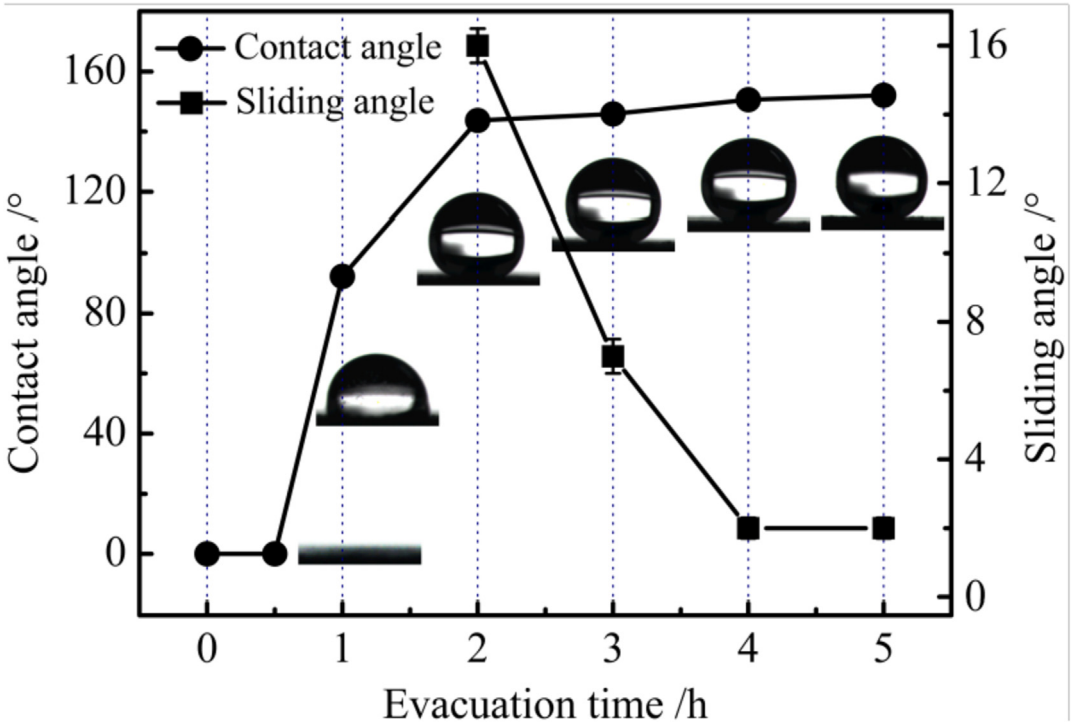

Fig. 5. The variation schematic of water contact angle and sliding angle of the Ni20Cr coating surface after vacuum evacuation with different time. Inset images are showing the water contact angle corresponding to different evacuation time.

oxide [24]. Because of the high temperature of plasma jet and the large amounts of oxygen in ambient air, plasma spraying was accompanied by oxidation reactions of materials even with a shroud protection. Oxides mainly formed during the in-flight stage after leaving the shroud and the post-depositional stage [25]. Hydroxyls were also detected on the as-sprayed surface, where the broad band around 3400 cm^{-1} was assigned to hydrogen bonding of O-H [26]. It is reported that metallic oxides are often covered with OH groups [27]. Since the surface free energy of hydroxyl and metal oxide is higher than that of water (72.8 mN m^{-1} at ~22 °C), combined with the capillary effect caused by the rough hierarchical structure, the as-sprayed coating surface presented super-hydrophilicity in the initial state [28,29].

As shown in Fig. 6a, the variation of each coating surface after vacuum evacuation with different time was evaluated by comparing the spectral results obtained after normalization. Some strong new peaks appeared on the surface and the peak intensity gradually increased with the extension of evacuation time, indicating that the content of these functional groups gradually increased.

Fig. 6(b and c) show the absorbance spectra of the coating surface after 5 h of evacuation. In the high-frequency region around 3000 cm^{-1}, two peaks at 2926 cm^{-1} and 2856 cm^{-1} were attributed to the asymmetric and symmetric stretching vibrations of the CH_2 in the saturated hydrocarbons, respectively. The peak at 2960 cm^{-1} was assigned to the symmetric stretching vibration of the CH_3 group at the terminal of the saturated hydrocarbon chain [30,31]. The weak peaks detected in 1462, 1370, and 1309 cm^{-1} correspond to the CH_3 asymmetric deformation, CH_3 symmetric deformation, and CH_2 off-plane coiling vibration (Fig. 6c). The results showed that saturated hydrocarbon chain-containing substances or saturated hydrocarbons might appear on the coating surface.

In the low-frequency region, another two strong new peaks were observed at 1554 cm^{-1} and 1416 cm^{-1}, which were ascribed to the asymmetric and symmetric stretching absorptions of the carboxyl (COO), respectively. This demonstrated the formation of carboxylates on the surface after the evacuation process [11]. According to the reports [32,33], the frequency separation $\Delta\nu = \nu_{as}(COO)\text{-}\nu_s(COO)$ can elucidate the coordination mode of the carboxylates. The carboxylates with the value of $\Delta\nu$ closed to 150 cm^{-1} should belong to bidentate bridging complexes. Since only the absorption peaks related to saturated hydrocarbon groups were detected in addition to the carboxyl group, the terminal chain of the carboxylate molecules should be a saturated hydrocarbon chain.

According to the above results, the emerging absorption peak indicated that the carboxylates should exist on the coating surface after vacuum evacuation, while the existence of alkanes on the surface need further discussion in Section 3.5.

It has been reported that the surface free energy of hydrocarbon-only chain was as low as 24 mN m^{-1} [12]. In general, the number of carbon atoms in the hydrocarbon chain exceeds 10 can provide hydrophobic property. As a result, the wettability transition of the coating surface after the evacuation thanks to the newly emerging hydrophobic saturated hydrocarbon chains. With the increase of their content, the surface wettability gradually changed from super-hydrophilicity to super-hydrophobicity.

3.4. The source of the surface adsorbates

In order to further clarify the source of the adsorbates on the coating surface during vacuum evacuation process and to investigate whether the reasons for the surface wettability transition in different oil-free vacuum systems were the same, the XPS equipment operating under ultra-high vacuum conditions was used to carry out the relevant test.

An *in-situ* XPS test was designed to analyze the as-sprayed coating surface. During the process of *in-situ* XPS test, the coating surface was subjected to argon ion etching for 30 s. Argon ion etching was used to remove a certain extent of the contaminants, especially the carbon-containing substances already adsorbed on the as-sprayed coating surface. After that, the sample was exposed in the continuous evacuated high vacuum chamber of XPS for a certain period of time up to 5 h. Fig. 7 shows the XPS survey spectra of the surface in two states: i) the initial stage after etching and ii) after the evacuation. Throughout the detection process, the same area on the coating surface was subjected to

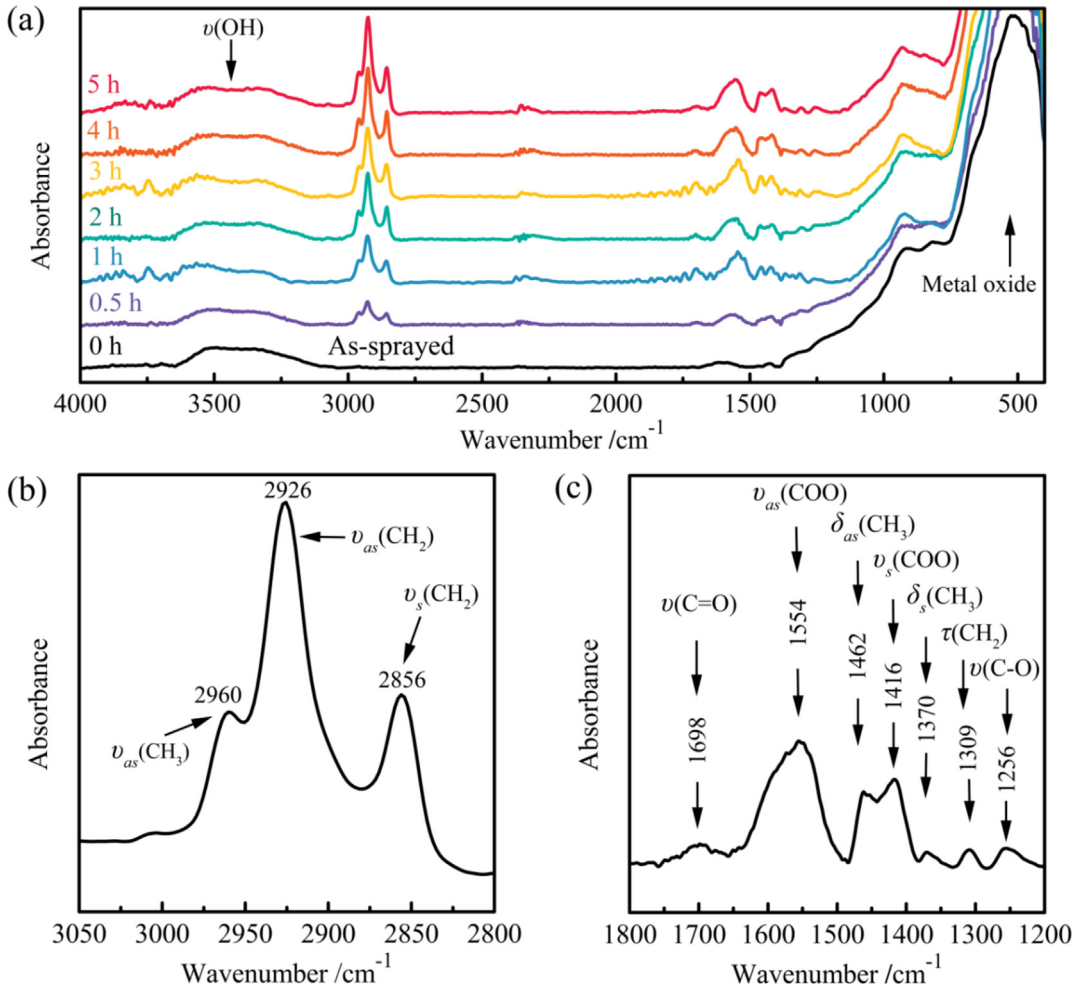

Fig. 6. DRIFTS absorbance spectra of the coating surfaces. (a) The evolution of absorbance spectra of the coating surface before (as-sprayed) and after vacuum evacuation with different time after normalization. (b, c) The absorbance spectra of the coating surface after vacuum evacuation treatment for 5 h.

detection.

From the results, the Ni20Cr coating surface was mainly made of Ni, Cr, O, and C element. The C atomic content relative to the metal (Ni and Cr) atomic content, represented by the atomic ratio C/M, was used to measure the relative content of adsorbed carbon-containing organic matter on the coating surface [34]. Comparing the proportions of each element between the two spectra, the ratio of C/M rose from 1.32 after argon ion etching to 2.34 after 5 h of evacuation, which indicated that the coating surface adsorbed the carbon-containing substances during the evacuation in the vacuum chamber. The results clearly demonstrated that the residual gas of carbon-containing substances existed in the vacuum system maintained by the oil-free vacuum pump, and the source of the emerging adsorbates on the surface were derived from the vacuum system.

The decomposition of the high-resolution C 1s and O 1s peaks were performed to further analyze the state of carbon-containing adsorbates on the surface. Fig. 8(a and b) represent the deconvoluted spectra from the C 1s, which were resolved into four contributions with binding energies of 284.6, 286.3, 287.5, and 289.0 eV, corresponding to C-C/C-H, C-O, C=O, and COO^-, respectively [16,34]. The O 1s spectra shown in Fig. 8(c and d) were resolved into three peaks centered at 530.9, 532.3, and 534.0 eV from M-O-M (the lattice oxygen), M-OH (the oxygen peak associated with hydroxyls) and COO^- (the oxygen peak associated with carboxyl), respectively [34].

From C 1s spectra of the coating surface after etching and evacuation, it was confirmed that the content of C-C/C-H was predominant. Therefore, with the increase of total carbon content after vacuum evacuation, the content of C-C/C-H increased on the surface as well. Moreover, obtaining from calculation of the spectral peak areas, the relative content of COO^- was 4.6% recorded for the etching state (Fig. 8a), increased to 8.7% after vacuum evacuation (Fig. 8b), which indicated that the adsorbates containing COO^- was accumulated on the surface during the evacuation. The O 1s spectra further confirmed the increase of COO^-. The relative content of COO^- was increased from 26.5% recorded in the etching state (Fig. 8c) to 33.1% after evacuation (Fig. 8d). The above result was consistent with the increase of the content of saturated hydrocarbon chains and carboxyl groups in DRIFTS spectra of the surface after evacuation in the SEM vacuum system.

Furthermore, the analysis of the contact angle and the DRIFTS on the coating surface after *in-situ* XPS detection was also carried out. The surface showed super-hydrophobicity. The absorption peaks appeared on the surface presented in Fig. 9 was consistent with that appeared on the surface experienced the evacuation in the SEM vacuum system. As a result, the substances spontaneous adsorbed on the surface who caused the wettability change was similar in different oil-free vacuum systems.

Based on the published reports [35], the volatile hydrocarbons and their derivatives exist everywhere in air and their concentration is typically parts-per-million. In the oil-free vacuum systems, the hydrocarbons and their derivatives may be introduced from the air since the chamber has to be opened during the sample exchange. In vacuum systems, they can present in gaseous form or be adsorbed on the inner walls of the chamber. Due to their low vapor pressure, they are difficult to extract in the vacuum space [36]. In addition, the substances adsorbed on the inner wall of the chamber will also gradually release with

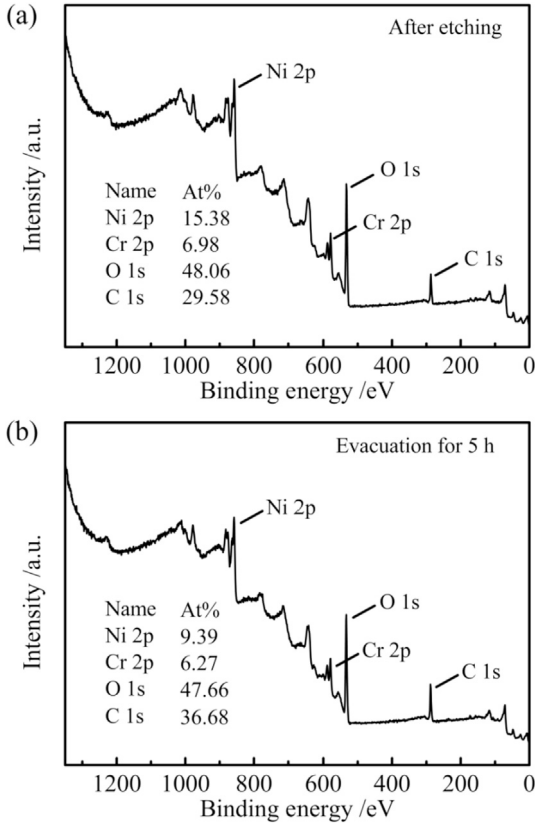

Fig. 7. Survey spectra and element content detected by *in-situ* XPS test on the as-sprayed coating surface. The surface (a) immediately after argon ion etching and (b) after the continuous evacuation for 5 h.

evacuation. Roediger et al. [37] have confirmed the presence of hydrocarbons in an oil-free SEM vacuum system by the detection through mass spectrometry. Therefore, hydrocarbon contamination was unavoidable in high vacuum or ultra-high vacuum, although the entire

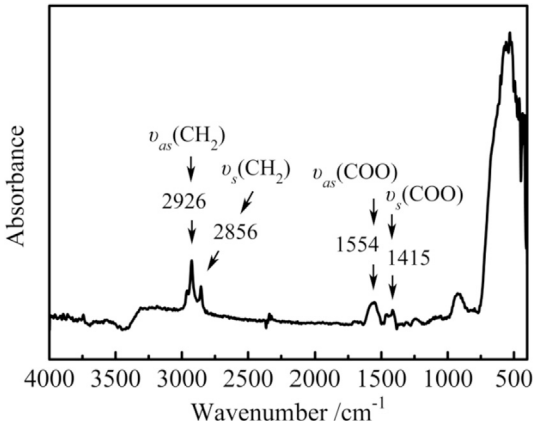

Fig. 9. The DRIFTS spectrum of the coating surface after evacuation in the XPS vacuum chamber for 5 h.

system was designed to be oil-free and hermetically sealed [38]. Since these residual gases were derived from the air, the surface adsorbates in different oil-free vacuum systems were similar.

3.5. The mechanism of spontaneous adsorption

As a comparison, the coating surface was placed in the SEM vacuum chamber for 5 h without continuous evacuation. When the chamber pressure was reduced to lower than 1×10^{-2} Pa, the vacuum pump was closed and the vacuum system entered standby mode. The chamber pressure was increased to 1×10^{-1} Pa during the sample placement. After the above process, the coating surface still showed super-hydrophilicity with a contact angle of 0°. The result reflected that the content of the adsorbates on the surface was not sufficient to cause a greater change in surface wettability. It also showed that the continuous evacuation in the vacuum system can accelerate the spontaneous adsorption on the surface.

The mechanism of spontaneous adsorption on the coating surface during vacuum evacuation was shown in Fig. 10. From the result of

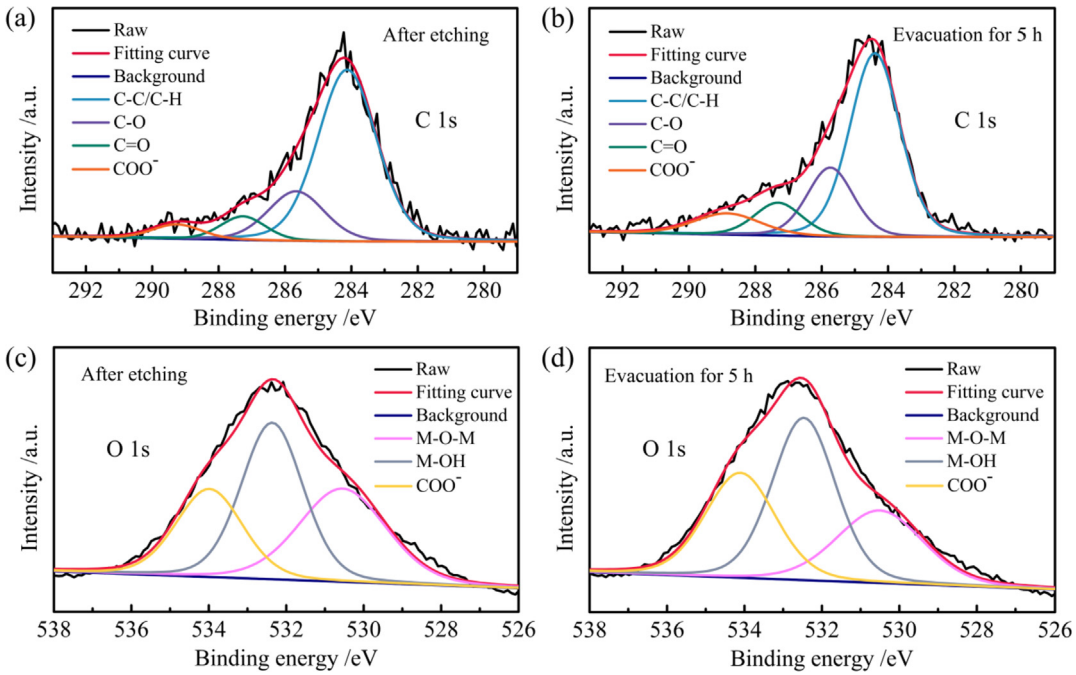

Fig. 8. Deconvolution of the XPS C 1s of the as-sprayed coating surface (a) immediately after argon ion etching and (b) after the continuous evacuation for 5 h. Deconvolution of the XPS O 1s of the as-sprayed coating surface (c) immediately after argon ion etching and (d) after the continuous evacuation for 5 h.

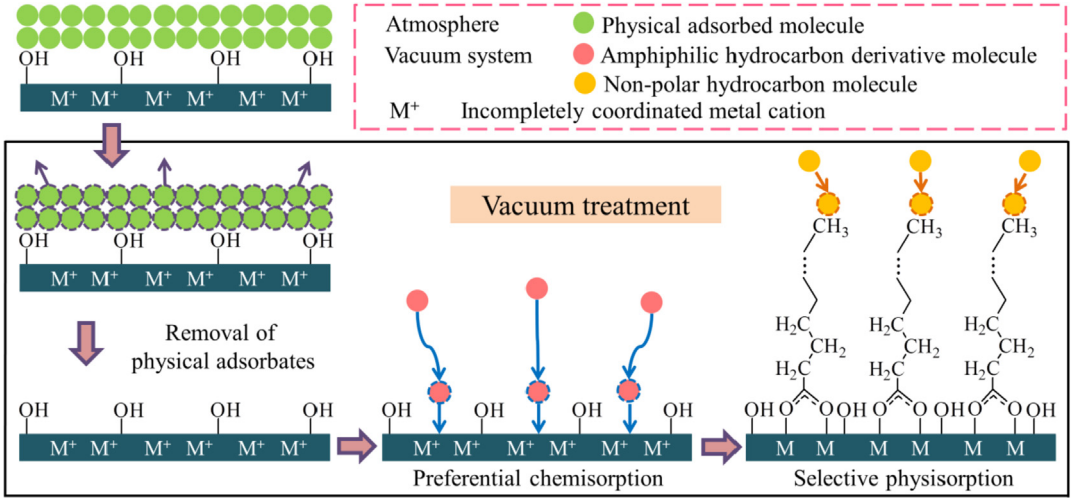

Fig. 10. Schematic diagrams of the spontaneous adsorption process on the coating surface during vacuum evacuation.

DRIFTS shown in Fig. 6a, the freshly as-sprayed coating surface contained oxides and hydroxyl groups, which showed a polar nature. Due to the presence of a large number of polar molecules in air, physical adsorption layers will form on the coating surface consisted of water, organic contaminants, and other compounds based on carbon, oxygen and sulfur [39]. The physical adsorption layers enabled the surface to be in a relatively stable state. New substances must replace or cover the existing physical adsorbed molecules that can make the adsorption process occur, thus the adsorption rate was very low under normal conditions.

During the continuous evacuation process in this study, physical adsorbates on the coating surface can be desorbed from the viewpoint of adsorption theory [40]. Once the surface was placed in a vacuum chamber with evacuation, desorption of physical adsorbates occurred, the balance of the surface was broken, the surface became unstable. The surface has to adsorb new substances to reduce its surface energy and recover the stability immediately [29]. Therefore, evacuation process broke the equilibrium state of the surface, causing the spontaneous adsorption on the surface and also improving the speed of adsorption process.

As can be seen from Figs. 6a and 8(c, d), the content of hydroxyl groups on the coating surface almost no changed after the vacuum evacuation. The results showed that vacuum evacuation treatment can only remove the physical adsorbates on the surface, while the hydroxyl groups presented on the surface by chemical bonding were difficult to be desorbed during the evacuation process. Therefore, when desorption of physical adsorption layers occurred, the oxides and the hydroxyls with polar nature directly exposed to the vacuum environment.

Saturated hydrocarbons are non-polar molecules. Since non-polar molecules and their heterosexual molecules are mutually exclusive, theoretically saturated hydrocarbon molecules cannot preferentially adsorb on the coating surface at the initial stage during vacuum evacuation.

The results of DRIFTS and XPS detection demonstrated that the carboxylates containing saturated hydrocarbon chains existed on the coating surface during vacuum evacuation. According to these adsorbates, it can be speculated that they were formed based on the acid-base reaction between metal ions and amphiphilic saturated hydrocarbon derivatives [41]. The weak stretching vibration of carbonyl (C=O) and C-OH appeared on the evacuation treated surface (Fig. 6c), and the content of C-O and C=O from the deconvolution of the C 1s increased on the surface after vacuum evacuation (Fig. 8a, b) further proof the existed of the unreacted hydrocarbon derivatives.

It has been reported that incompletely coordinated metal cations usually exist on the metal oxide surface. Nanostructures with a large number of defects on the coating surface can cause the surface having many incompletely coordinated metal cations. Metal cations have a strong electron-accepting nature. Aliphatic compounds such as ester and carboxylic acid can react with these sites spontaneously and form the chemisorbed carboxylates [41,42]. Therefore, when the physical adsorption layers were removed by evacuation, metal cations on the oxide surface were directly exposed to the vacuum. The amphiphilic hydrocarbon derivative molecules from the vacuum residual gas can spontaneously undergo chemical adsorption on the surface.

Meanwhile, due to the exposure of polar oxides and hydroxyl groups on the surface, other polar residual gas molecules in vacuum can also be attracted to physically adsorb through van der Waals forces or hydrogen bonds. However, their binding forces are relatively weak. The physical adsorbed molecules can easily be desorbed and replaced by other molecules. Therefore, the amphiphilic hydrocarbon derivatives will preferentially adsorb on the surface to form a stable monolayer carboxylate adsorption layer based on the driving force of the chemical reaction.

Further, the results of DRIFTS in Fig. 6a showed that when vacuum evacuation was applied for more than 2–3 h, the content of the carboxyl groups on the surface was no longer changed with time. This is due to the fact that the chemically adsorbed carboxylate on the surface belongs to monolayer adsorption. When the reaction sites were exhausted, the content of carboxylate adsorption will reach saturation. However, DRIFTS results showed that the content of hydrocarbon groups having a continuously increasing trend. This indicated that in addition to the saturated hydrocarbon chains in the carboxylates through chemisorption, the surface was also accompanied by physisorption of saturated hydrocarbons during vacuum evacuation. Since the saturated hydrocarbon chains in the preferentially adsorbed monomolecular carboxylate are non-polar, they extend outward from the surface, affecting not only the surface wettability but also the subsequent adsorption behavior of the surface. Non-polar saturated hydrocarbon chains can adsorb non-polar residual gas molecules to form subsequent physical adsorption layers. Therefore, under the effect of chemisorption and subsequent physisorption, the coating surface can preferentially adsorb residual gas molecules containing hydrophobic hydrocarbon groups in vacuum, which led to the change in surface wettability.

Based on the above analysis, it is worth emphasizing that the adsorption on the metal oxide surfaces during vacuum evacuation was an inevitable phenomenon and has a strong selectivity feature.

3.6. *Reversible wettability transition of the coating surface*

It was found that when the prepared super-hydrophobic coating

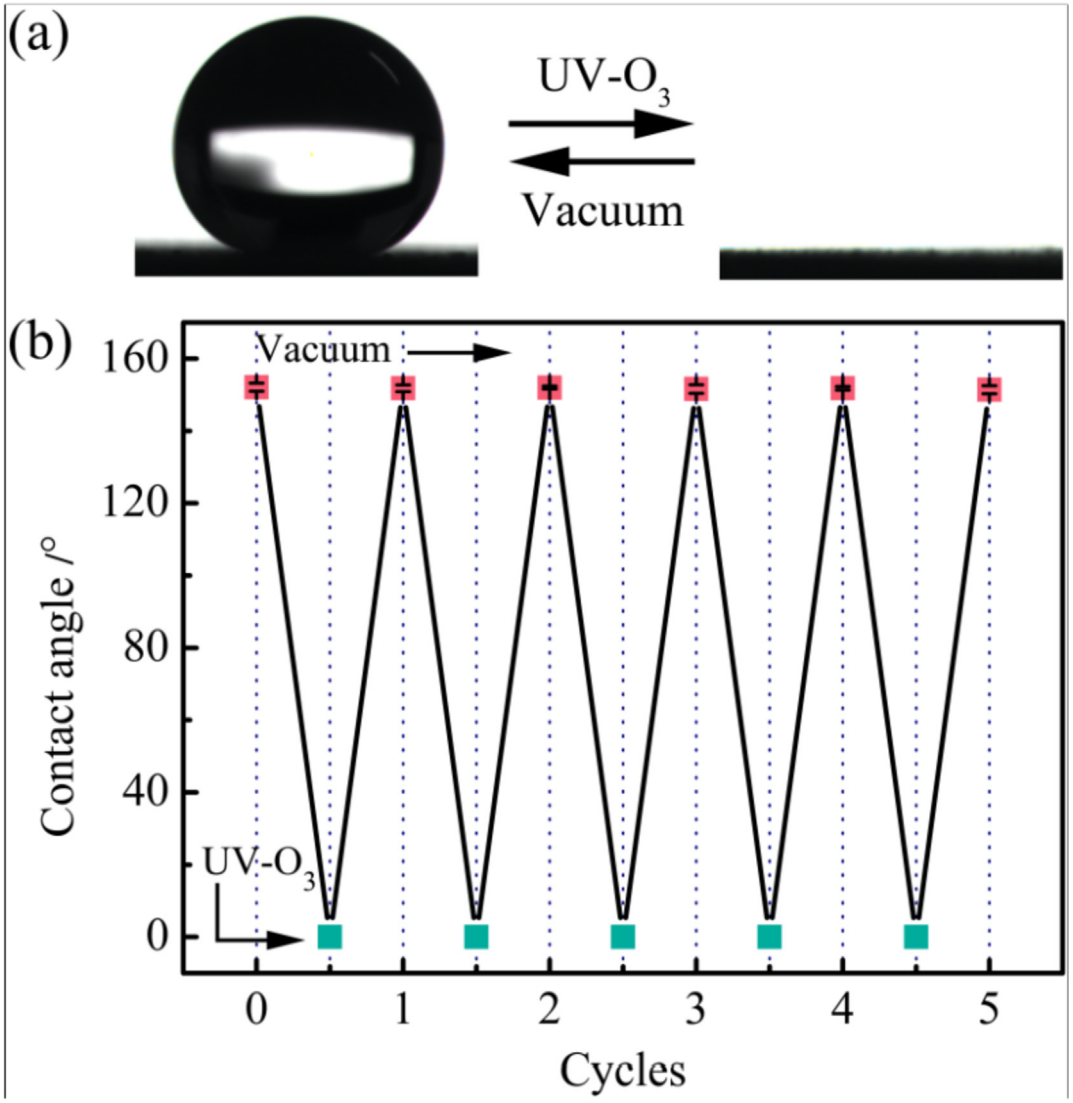

Fig. 11. Reversible wettability transition of the coating surface. (a) Images of a water droplet on the coating surface after vacuum evacuation and UV-O_3 treatment, respectively. (b) Switching between super-hydrophobicity and super-hydrophilicity on the coating surface through vacuum evacuation and UV-O_3 treatment.

surface by vacuum evacuation was irradiated in a UV-O_3 device for 1 h, the surface can be restored to the original super-hydrophilic state. After evacuation in the vacuum for 5 h again, the surface was able to recover the super-hydrophobicity. This process can be repeated several times as shown in Fig. 11. The coating surface showed a good reversible transition between super-hydrophobicity and super-hydrophilicity by vacuum evacuation and UV-O_3 treatment.

Through the observation, surface morphology was not damaged by UV-O_3 treatment. Analysis showed that the super-hydrophobicity was attributed to the adsorbates containing saturated hydrocarbon chain on the coating surface. Therefore, the disappearance of the hydrophobic performance was due to the loss of these hydrophobic functional groups by UV-O_3 treatment. During the UV-O_3 treatment, the ozone from the air can be decomposed to the active oxygen atoms with strong oxidizing property, who was able to oxidize the adsorbates especially the hydrocarbon chains on the surface and generated CO, CO_2, H_2O and so on [43]. When the surface was subjected to vacuum evacuation again, some residual physisorbed substances formed by UV-O_3 treatment on the surface can be removed. Then, the exposed metal oxides can selectively spontaneous adsorb the residual gas in the vacuum again, leading the surface obtained super-hydrophobicity.

3.7. Stability of the super-hydrophobic surface

Stability of the super-hydrophobic coating surface has a significant impact on the practical applications. To evaluate the stability, the coating was exposed for about one month in an outdoor environment at a temperature range from −9 to 13 °C and a relative humidity of 23%–92%.

Fig. 12 depicts the variation of both the contact angle and the sliding angle of the surface at different exposure times. Slight fluctuation occurred on the super-hydrophobicity of the surface, demonstrating the long-term stability of the treated surface under the external environment. After the evacuation treatment, non-polar molecules were adsorbed on the outmost layer of the super-hydrophobic coating surface. The exposition of the coating to the atmosphere repelled polar molecules, such as water vapor, prevented re-adsorption of hydrophilic substances. Therefore, the surface could maintain the super-hydrophobic state.

4. Conclusions

In the present paper, the mechanism of wettability transition on the Ni20Cr coating surface in the devices working under vacuum system

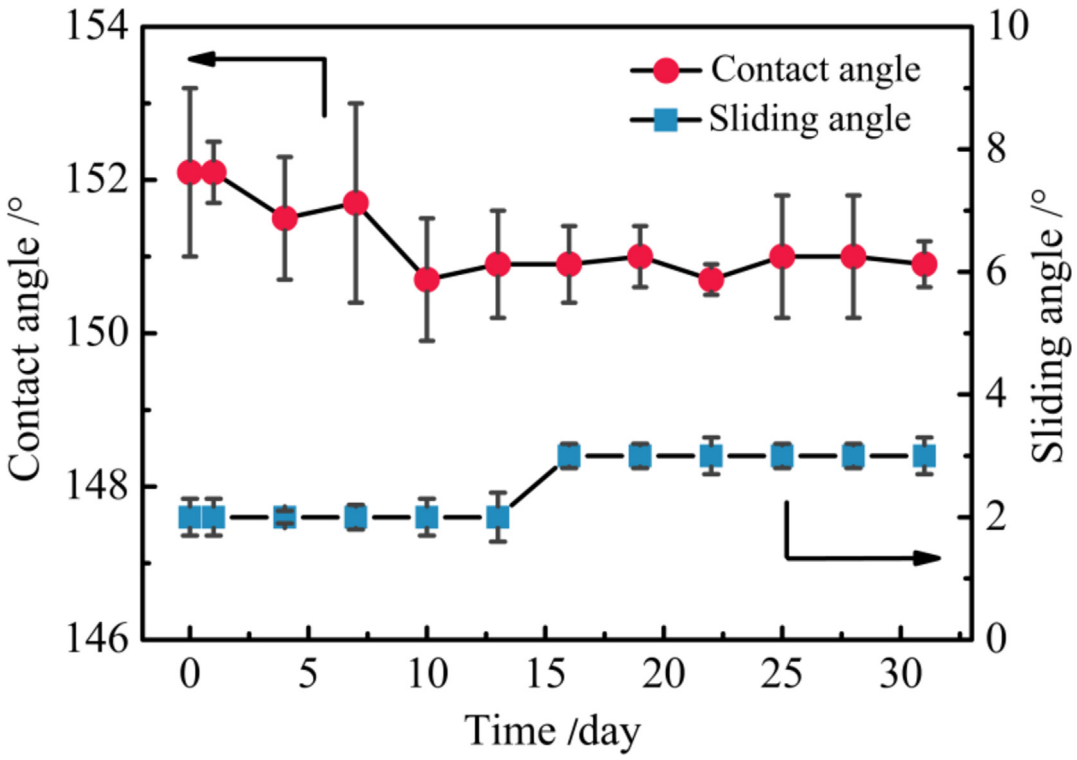

Fig. 12. The variation of water contact angle and sliding angle of the super-hydrophobic surface as a function of time when exposed in the outside environment.

has been clarified. The transition was attributed to the formation of chemisorbed carboxylates containing hydrophobic saturated hydrocarbon chains and physisorbed saturated hydrocarbons on the coating surface through the selective spontaneous adsorption from the vacuum residual gas molecules, while evacuation process enhanced the adsorption rate. With this work, we understood more about the impact of the vacuum conditions for the surface wettability. In different oil-free vacuum systems, the spontaneous adsorption of the metal oxide surface was unavoidable, while the adsorption process was selective and the surface adsorbates were similar. Based on the adsorption and desorption of the surface adsorbates, the coating surface had a good reversible transition between super-hydrophobicity and super-hydrophilicity through vacuum evacuation and UV-O_3 treatment. Furthermore, the coating with super-hydrophobicity showed a long-term stability under outdoor conditions.

Funding

This work was supported by the National Basic Research Program of China [2012CB625100].

Acknowledgments

The authors acknowledged the funding support from the National Basic Research Program of China [2012CB625100].

References

[1] X. Zhang, F. Shi, J. Niu, Y. Jiang, Z. Wang, Superhydrophobic surfaces: from structural control to functional application, J. Mater. Chem. 18 (2008) 621–633.
[2] B. Bhushan, Y.C. Jung, Natural and biomimetic artificial surfaces for superhydrophobicity, self-cleaning, low adhesion, and drag reduction, Mater. Sci. 56 (2011) 1 108.
[3] F. Xiao, S. Yuan, B. Liang, G. Li, S.O. Pehkonenc, T. Zhang, Superhydrophobic CuO nanoneedle-covered copper surfaces for anticorrosion, J. Mater. Chem. 3 (2015) 4374–4388.
[4] H.J. Ensikat, P. DitscheKuru, C. Neinhuis, W. Barthlott, Superhydrophobicity in perfection: the outstanding properties of the lotus leaf, Beilstein J. Nanotechnol. 2 (2011) 152–161.
[5] L. Feng, S. Li, Y. Li, H. Li, L. Zhang, Y. Song, B. Liu, L. Jiang, D. Zhu, Super-hydrophobic surfaces: from natural to artificial, Adv. Mater. 14 (2002) 1867 1860.
[6] J.M. Lim, G.R. Yi, J.H. Moon, C.J. Heo, S.M. Yang, Superhydrophobic films of electrospun fibers with multiple-scale surface morphology, Langmuir 23 (2007) 7981–7989.
[7] L. Zhao, Q. Liu, R. Gao, J. Wang, W. Yang, L. Liu, One-step method for the fabrication of superhydrophobic surface on magnesium alloy and its corrosion protection, antifouling performance, Corrosion Sci. 80 (2014) 177–183.
[8] M. Ruan, W. Li, B. Wang, B. Deng, F. Ma, Z. Yu, Preparation and anti-icing behavior of superhydrophobic surfaces on sluminum slloy substrates, Langmuir 29 (2013) 8482–8491.
[9] C. Gao, Z. Sun, K. Li, Y. Chen, Y. Cao, S. Zhang, L. Feng, Integrated oil separation and water purification by a double-layer TiO_2-based mesh, Energy Environ. Sci. 6 (2013) 1147–1151.
[10] C. Barbe, J. Bartlett, L. Kong, K. Finnie, H.Q. Lin, M. Larkin, S. Calleja, A. Bush, G. Calleja, Silica partical: a novel drug-delivery system, Adv. Mater. 16 (2004) 1959–1966.
[11] S. Alexander, J. Eastoe, A.M. Lord, F. Guittard, A.R. Barron, Branched hydrocarbon low surface energy materials for superhydrophobic nanoparticle derived surfaces, ACS Appl. Mater. Interfaces 8 (2016) 660–666.
[12] M. Sagisaka, T. Narumi, M. Niwase, S. Narita, A. Ohata, C. James, A. Yoshizawa, E.T. de Givenchy, F. Guittard, S. Alexander, J. Eastoe, Hyperbranched hydrocarbon surfactants give fluorocarbon-like low surface energies, Langmuir 30 (2014) 6057–6063.
[13] L. Martínez, E. Román, J.L. de Segovia, S. Poupard, J. Creus, F. Pedraza, Surface study of cerium oxide based coatings obtained by cathodic electrodeposition on zinc, Appl. Surf. Sci. 257 (2011) 6202–6207.
[14] F. Pedraza, S.A. Mahadik, B. Bouchaud, Synthesis of ceria based superhydrophobic coating on Ni20Cr substrate via cathodic electrodeposition, Phys. Chem. Chem. Phys. 17 (2015) 31750–31757.
[15] B. Yan, J. Tao, C. Pang, Z. Zheng, Z. Shen, C.H.A. Huan, T. Yu, Reversible UV-light-induced ultrahydrophobic-to-ultrahydrophilic transition in an α-Fe_2O_3 nanoflakes film, Langmuir 24 (2008) 10569–10571.
[16] J. Long, M. Zhong, P. Fan, D. Gong, H. Zhang, Wettability conversion of ultrafast laser structured copper surface, J. Laser Appl. 27 (2015) S29107.
[17] P. Bhattacharya, S. Gohil, J. Mazher, S. Ghosh, P. Ayyub, Universal, geometry-driven hydrophobic behaviour of bare metal nanowire clusters, Nanotechnology 19 (2008) 075709.
[18] M. Pei, B. Wang, E. Li, X. Zhang, X. Song, H. Yan, The fabrication of super-hydrophobic copper films by a low-pressure-oxidation method, Appl. Surf. Sci. 256 (2010) 5824–5827.
[19] G. Li, B. Wang, Y. Liu, T. Tan, X. Song, H. Yan, Fabrication of superhydrophobic ZnO/Zn surface with nanowires and nanobelts structures using novel plasma assisted thermal vapor deposition, Appl. Surf. Sci. 255 (2008) 3112–3116.
[20] S. Matthews, Shrouded plasma spray of Ni-20Cr coatings utilizing internal shroud film cooling, Surf. Coat.Tech 249 (2014) 56–74.

[21] B. Vautherin, M.P. Planche, R. Bolot, A. Quet, L. Bianchi, G. Montavon, Vapors and droplets mixture deposition of metallic coatings by very low pressure plasma spraying, J. Therm. Spray Technol. 23 (2014) 596–608.
[22] J. Li, C.X. Li, G.J. Yang, C.J. Li, Effect of vapor deposition in shrouded plasma spraying on morphology and wettability of the metallic Ni20Cr coating surface, J. Alloy. Comp. 735 (2018) 430–440.
[23] W. Barthlott, C. Neinhuis, Purity of the sacred lotus, or escape from contamination in biological surfaces, Planta 202 (1997) 1–8.
[24] X. Chen, J. Yuan, J. Huang, K. Ren, Y. Liu, S. Lu, H. Li, Large-scale fabrication of superhydrophobic polyurethane/nano-Al_2O_3 coatings by suspension flame spraying for anti-corrosion applications, Appl. Surf. Sci. 311 (2014) 864–869.
[25] Q. Wei, Z. Yin, H. Li, Oxidation control in plasma spraying NiCrCoAlY coating, Appl. Surf. Sci. 258 (2012) 5094–5099.
[26] G. Verma, S.K. Dhoke, A.S. Khanna, Polyester based-siloxane modified waterborne anticorrosive hydrophobic coating on copper, Surf. Coating. Technol. 212 (2012) 101–108.
[27] D. Cappus, C. Xu, D. Ehrlich, B. Dillmann, C.A. Ventnce Jr., K. Al Shamery, H. Kuhlenbeck, H.J. Freund, Hydroxyl groups on oxide surfaces: NiO(100), NiO(lll) and Cr2O3(111), Chem. Phys. 177 (1993) 533–546.
[28] S. Takeda, M. Fukawa, Y. Hayashi, K. Matsumoto, Surface OH group governing adsorption properties of metal oxide films, Thin Solid Films 339 (1999) 220–224.
[29] J. Drelich, E. Chibowski, D.D. Meng, K. Terpilowski, Hydrophilic and superhydrophilic surfaces and materials, Soft Matter 7 (2011) 9804–9828.
[30] L.B. Boinovich, A.M. Emelyanenko, A.S. Pashinin, C.H. Lee, J. Drelich, Y.K. Yap, Origins of thermodynamically stable superhydrophobicity of boron nitride nanotubes coatings, Langmuir 28 (2012) 1206–1216.
[31] S.H. Lee, Z.R. Dilworth, E. Hsiao, A.L. Barnette, M. Marino, J.H. Kim, J.G. Kang, T.H. Jung, S.H. Kim, One-step production of superhydrophobic coatings on flat substrates via atmospheric Rf plasma process using non-fluorinated hydrocarbons, ACS Appl. Mater. Interfaces 3 (2011) 476–481.
[32] Y. Qiao, Y. Lin, Y. Wang, Z. Yang, J. Liu, J. Zhou, Y. Yan, J. Huang, Metal-driven hierarchical self-assembled one-dimensional nanohelices, Nano Lett. 9 (2009) 4500–4504.
[33] W. Xu, Y. Hu, W. Bao, X. Xie, Y. Liu, A. Song, J. Hao, Superhydrophobic copper surfaces fabricated by fatty acid soaps in aqueous solution for excellent corrosion resistance, Appl. Surf. Sci. 399 (2017) 491–498.
[34] J. Long, M. Zhong, H. Zhang, P. Fan, Superhydrophilicity to superhydrophobicity transition of picosecond laser microstructured aluminum in ambient air, J. Colloid Interface Sci. 441 (2015) 1–9.
[35] P. Liu, L. Cao, W. Zhao, Y. Xia, W. Huang, Z. Li, Insights into the superhydrophobicity of metallic surfaces prepared by electrodeposition involving spontaneous adsorption of airborne hydrocarbons, Appl. Surf. Sci. 324 (2015) 576–583.
[36] H.D. Wanzenboeck, P. Roediger, G. Hochleitner, E. Bertagnolli, Novel method for cleaning a vacuum chamber from hydrocarbon contamination, J. Vac. Sci. Technol. 28 (2010) 1413–1420.
[37] P. Roediger, H.D. Wanzenboeck, G. Hochleitner, E. Bertagnolli, Evaluation of chamber contamination in a scanning electron microscope, J. Vac. Sci. Technol. B 27 (2009) 1071 1023.
[38] V.I. Perekrestov, S.N. Kravchenko, Change in the composition of residual gases in a vacuum chamber during Ti film deposition, Instrum. Exp. Tech. 45 (2002) 404–407.
[39] E. McCafferty, J.P. Wightman, Determination of the concentration of surface hydroxyl groups on metal oxide films by a quantitative XPS method, Surf. Interface Anal. 26 (1998) 549–564.
[40] S.J. Lombardo, A.T. Bell, Monte Carlo simulations of the effect of pressure on isothermal and temperature-programmed desorption kinetics, Surf. Sci. 245 (1991) 213–224.
[41] A. Ulman, Formation and structure of self-sssembled monolayers, Chem. Rev. 96 (1996) 1533–1554.
[42] J. van den Brand, O. Blajiev, P.C.J. Beentjes, H. Terryn, J.H.W. de Wit, Interaction of ester functional groups with aluminum oxide surfaces studied using infrared reflection absorption spectroscopy, Langmuir 20 (2004) 6318–6326.
[43] S. Lei, F. Wang, W. Li, G. Qiao, Reversible wettability between superhydrophobicity and superhydrophilicity of Ag surface, Sci. China Mater 59 (2016) 348–354.